Supplementary Appendix

This appendix has been provided by the authors to give readers additional information about their work.

Supplement to: Has C, Spartà G, Kiritsi D, et al. Integrin α_3 mutations with kidney, lung, and skin disease. N Engl J Med 2012;366:1508-14.

SUPPLEMENTARY APPENDIX

Integrin α3 Mutations with Kidney, Lung and Skin Disease

Cristina Has, M.D., Giuseppina Spartà, M.D., Dimitra Kiritsi, M.D., Lisa Weibel, M.D., Alexander Moeller, M.D., Virginia Vega-Warner, Ph.D., Aoife Waters, M.D., Yinghong He, M.D., Yair Anikster, M.D. Ph.D., Philipp Esser, Ph.D., Beate Straub, M.D., Ingrid Hausser, Ph.D., Detlef Bockenhauer, M.D. Ph.D., Benjamin Dekel M.D. Ph.D., Friedhelm Hildebrandt, M.D., Leena Bruckner-Tuderman, M.D., and Guido F. Laube, M.D.

LIST OF CONTENTS

SUPPLEMENTARY METHODS

Genetic Analysis

Mutation analysis of *ITGA3* was performed in Patient 1 based on a candidate gene approach, as described in Results. Thereafter, 10 patients with unclear forms of EB and eight families with focal segmental glomerulosclerosis and homozygosity at the *ITGA3* locus[1] were screened for mutations. Genomic DNA was extracted from peripheral-blood leukocytes using QIAmp® DNA mini kit (QIAGEN, Hilden, Germany). The coding exons and the exon / intron boundaries of the gene for integrin α3 (*ITGA3*) were amplified by PCR using primers designed with Primer3 Software (version 0.4.0) (Supplementary Table 3). All PCR products were submitted to automated nucleotide sequencing in an ABI 3130XL genetic analyzer using Big Dye Terminator Chemistry (Applied Biosystems, Darmstadt, Germany). DNA sequences were compared to the reference sequence from NCBI Entrez Nucleotide database (NC_000017.10) using Mutation Surveyor™ DNA variant analysis software (version 2.61 Softgenetics, State College, PA, USA). After written informed consent, EDTA-blood for DNA extraction was obtained from ethnically matched controls. Because the mutation found in Patient 1 abrogates the restriction site of Sac I, restriction length polymorphism was used for screening of 100 Southern Italian control chromosomes. The mutations found in Patient 2 and 3 were screened by direct sequencing of PCR products, and were excluded from 200 Palestinian-Arab and 136 Pakistani control chromosomes, respectively.

Mutation analysis of the *NPHS2* and *WT1,* genes was performed using heteroduplex analysis and direct sequencing as described before.[2-4] *CFTR* mutations were analysed using two commercially available CF-gene mutations kits: INFINITI® CFTR-15 Assay (AutoGenomics, Vista, USA), which tests for 15 *CFTR* mutations, and LUMINEX xTAG® Cystic Fibrosis 39 kit v2 (Luminex Corporation, Austin, USA), which tests for 39 *CFTR* mutations. *ABCA3* was analysed by PCR and direct sequencing of the entire coding region.[5]

Morphological Analyses of Skin, Kidney and Lung

For histopathological examination with light microscopy, skin, kidney and lung biopsy specimens were embedded in paraffin, and the sections were stained with haematoxylin and eosin (H&E) by standard procedures.

Immunohistochemistry was performed using the AEC (3-amino-9-ethylcarbazole) system (Dako, Hamburg, Germany) and haematoxylin as the counter stain. The primary antibodies used are listed in Supplementary Table 4. Control tissues were from newborns/infants.

Indirect immunofluorescence staining of the skin was performed on 5 µm cryosections, which were air dried and incubated with primary antibodies overnight at 4°C as described before.[6] The primary antibodies used are listed in Supplementary Table 4. The mouse monoclonal antibody P1B5 was used to specifically detect human integrin α3,[7, 8] which consists of 1051 amino acids and has a calculated molecular mass of 116 kDa (observed molecular mass of 130 kDa on SDS-PAGE under reducing conditions). The secondary antibodies were Alexa-488 anti-mouse or anti-rabbit IgG (both Invitrogen, Darmstadt, Germany). Nuclei were stained with DAPI (4',6-diamidino-2-phenylindole) (Millipore, Temecula, CA, USA). The stained sections were observed with a confocal laser scanning microscope (LSM510, Carl Zeiss, Jena, Germany).

For TEM analysis, the biopsies were fixed for at least 2h at room temperature in 3% glutaraldehyde solution in 0.1M cacodylate buffer pH 7.4, cut into pieces of ca. 1mm^3, washed in buffer, postfixed for 1 h at 4^{o}C in 1% osmium tetroxide, rinsed in water, dehydrated through graded ethanol solutions, transferred into propylene oxide, and embedded in epoxy resin (glycidether 100). Semithin and ultrathin sections were cut with an ultramicrotome (Reichert Ultracut E). Ultrathin sections were treated with uranyl acetate and lead citrate, and examined with a Zeiss EM 900 electron microscope.

In Vitro Studies of Integrin α3 Null Keratinocytes

Primary keratinocytes from control and Patient's 1 skin were isolated and cultivated in keratinocyte growth medium (Invitrogen) as described.[6] For flow cytometry analysis to detect α2, α3, α6, and β1 integrin subunits on the cell surface, $2x10^5$ cells were trypsinized, washed twice with PBS (phosphate buffered saline), and then incubated with the primary antibodies (Supplementary Table 4) for 15 minutes at room temperature. After washing with PBS containing 1% BSA (bovine serum albumin*)* and 0.05% sodium azide, the cells were incubated with FITC (fluoresceinisothiocyanat) conjugated $F(ab')_2$ goat anti-mouse of anti rat IgG(H+C) antibody (Immunotech, PN) for further 15 minutes. In a parallel experiment isotype controls were used. Flow cytometry acquisition was performed using the BD FACSCanto™II (BD Biosciences, Oxford, UK).

SUPPLEMENTARY RESULTS

In the skin of Patient 1, the disorganized basement membrane was associated with cellular abnormalities. In the epidermis, the basal keratinocytes were irregular in shape, rather than polyhedral columnar as in the normal skin (Supplementary Fig. 7B, C). However, the cell-cell contacts were not affected, as shown by β-catenin staining (Supplementary Fig. 7C). Cell proliferation, as assessed by Ki67 staining, was comparable to controls (Supplementary Fig. 8A). There was a mild infiltration of CD3 positive inflammatory cells, but no evidence for CD4, CD8, CD20 or CD68 positive infiltrates (Supplementary Fig. 8B). These findings are very similar to the data derived from the mouse model with epidermis-specific ablation of integrin α3.[9]

Because of the severe clinical lung involvement in our patients, transmission electron microscopy and immunohistochemistry were employed to uncover more subtle morphological changes. In agreement with the collagen IV staining, the transmission electron microscopy of the lung of Patient 1 revealed reduplications and irregularities of the alveolar basement membrane (Supplementary Fig. 9A). In Patient 2, abnormal lamellar bodies, the secretory organelles of type II alveolar cells involved in surfactant formation were noted (not shown). Immunohistochemistry for pro-surfactant protein C (pro-SPC) on the lung of Patient 1 demonstrated numerous type II alveolar pro-SPC-positive cells (Supplementary Fig. 9B). This is in accordance with the data derived from the mice with lung epithelial cell-specific loss of integrin α3.[10] The anomalies of the basement membrane are consistent with those observed in kidney and skin and presumably directly related to the genetic defect.

SUPPLEMENTARY TABLES

Supplementary Table 1. Patients, *ITGA3* Mutations, Clinical Features and Investigations

Clinical features / Investigations		Patients / *ITGA3* mutations / Origin Patient 1 c.1173_1174del p.Pro392ValfsX2 Southern Italy	Patient 2 c.1538-1G>A Gaza	Patient 3 c.1883G>C p.Arg628Pro Pakistan
Kidney	**Clinical and laboratory findings**	Congenital nephrotic syndrome Peritoneal dialysis	Congenital nephrotic syndrome Peritoneal dialysis	Congenital nephrotic syndrome Peritoneal dialysis
	Histology	Globally atrophic glomeruli, segmental glomerulosclerosis, diffuse interstitial fibrosis and tubular atrophy	Right: enlarged proximal tubules with cyst formation, focal segmental sclerosis; left: renal dysplasia	Focal segmental glomerulosclerosis
	Transmission electron microscopy	NA	Focal mesangial hyperplasia, podocyte effacement	Lamellation of the basement membranes
Lung	**Clinical features**	Respiratory distress, oxygen-dependent, aspiration pneumonia, recurrent respiratory infections	Respiratory distress, oxygen-dependent	Respiratory distress, oxygen-dependent, aspiration pneumonia, recurrent respiratory infections
	Chest radiograph	Interstitial reticulo-nodular changes	Bilateral infiltrates	Right upper and middle lobe pneumonia
	CT	Non-specific diffuse distortion of the pulmonary architecture consistent with interstitial lung disease	Diffuse interstitial changes consistent with diffuse lung disease	Diffuse interstitial changes consistent with interstitial lung disease
	Histology	Overinflation and mild-to-moderate simplification of airspaces[1]	Consistent with chronic pneumonitis of infancy probably superimposed on lung growth abnormality and associated with recent thromboembolism[2]	Interstitial fibrosis
	Transmission electron microscopy	Reduplicated and irregular alveolar basement membrane	Abnormal lamellar bodies in the alveolar cells	NA

Skin	**Clinical features**	Blisters, nail dystrophy	Persistent erosions on the buttocks	Blisters, nail dystrophy
	Immunomapping	Focal disruption of the dermal-epidermal junction, cleavage within the plane of the basement membrane	NA	Focal disruption of the dermal-epidermal junction
	Transmission electron microscopy	Thin lamina densa, discontinuous between the hemidesmosomes	NA	NA
Mutations were excluded in the following genes		*NPHS2, WT1, ABCA3*, frequent *CFTR* mutations	*NPHS1, NPHS2, WT1* (exons 8 and 9)	*NPHS2, WT1* (exons 8 and 9)
Other investigations		Laryngoscopy: normal findings Bronchoscopy: unremarkable Gastrointestinal tract biopsies: no significant abnormalities of the stomach and oesophagus, but the small intestine showed mild flattening of the villous epithelium Cerebral MRI at the age of one month: normal anatomy	Sweat test: normal Bronchoscopy: unremarkable Barium swallowing: unremarkable Brain ultrasound and CT: normal	NA

Legend: [1]an open lung biopsy was performed; [2]histopathology was performed postmortem; CT, computed tomography; NA, not available; MRI, magnetic resonance imaging.

Supplementary Table 2. Associated Features and Investigations in Patient 1

Birth measurements:		
• Weight (g)	4090 (90th percentile)	
• Height (cm)	53.5 (50-75th percentile)	
• Head circumference (cm)	34.5 (10-25th percentile)	
• Apgar	8/8/8	
• Umbilical arterial pH	7.25 (normal range 7.20-7.38)	
Clinical laboratory at day 13 of life before initiation of dialysis:		
Blood parameter	Value	Normal range
• Creatinine (mg/dl)	5.8	< 0.6
• Urea (mg/dl)	186	7.2 -42.0
• Albumin (g/dl)	1.6	> 3.5
• IgA (mg/dl)	<7	39 - 71
• IgG (mg/dl)	257	280 - 710
• IgM (mg/dl)	38	54 - 144
• Blood pH	7.21	7.35 - 7.45
• Base excess (mmol/l)	-15	-3 + 3
• Cholesterol (mg/dl)	387	62 - 189
• Triglyceride (mg/dl)	1314	19 - 85
Urine parameters		
• Protein/creatinine ratio (mg/mg)	12.5	< 0.9
GFR[1] ml/min/1.73 m^2	<10	40 - 60
Respiratory parameters with oxygen supplementation:		
• Venous CO_2 (kPa)	6.5 - 9.0	5.5 - 6.8
• Respiratory rate (/minute)	60 - 120	30 - 60
Other features:		
• Round face with prominent forehead, hypertelorism, antimongoloid slant, prominent nose with long saddle, small mouth, retrognathism, large ears		
• Narrow chest, gynecomastia		
• Discrete clinodactyly, deep furrows of the soles		
• Shrill cry		
• Swallowing and sucking reflexes present, although swallowing was repeatedly followed by cough and vomiting		
• Mild muscular hypotonia		
• Microcephaly		
• Delayed neurological development		
• Normal psycho-social interactions and cognitive development		
• Adenoviral enteritis and subsequent marked hepatosplenomegaly at the age of six months		

Legend: [1] Glomerular filtration rate (GFR) was estimated at day 13 of life by the Schwartz formula, using serum creatinine, height and a k constant of 0.4.

Supplementary Table 3. Primers Used for *ITGA3* Mutation Analysis

Exon	Primers	Product size (bp)
1	5'- gagagcgcagctgtgaaact 5'- cttaatcctggctcccaagg	497
2	5'- tgcctgccttaccctacact 5'- gaagcgactagaagccgtgt	397
3	5'- gctggatgggattggtagag 5'- cacaggaagggacatgtgtg	388
4	5'- ggagaaggagaagccaggag 5'- actggcatgaggtcctgttt	495
5	5'- atggcaaaatgctcaccaat 5'- atcttgggagcttggaacag	392
6	5'- gctggccatctggagtctac 5'- ctgcaaacctctgcaaacaa	492
7	5'- ggtgggtcatattggcatct 5'- ccccatcctgtctcatctgt	500
8	5'- catcaatcaggccaagatca 5'- cagtcccagcttctctccat	369
9	5'- ccccagcaggtacagagaga 5'- ccaggcttccaaggagcta	387
10	5'- ccatctgtgtccatgtttgc 5'- ttgggtagagagggcaaatg	337
11	5'- gtcagggacaccacagacct 5'- agaagaagccgtggaagaca	392
12	5'- agtgtgcaagtggagcttgtg 5'- tgtccccaacctctgtctct	396
13	5'- ggcgggtccagctcttct 5'- gcactccttctggaactgga	377
14	5'- caggctctggagaaccacac 5'- ttctgaccatcccacctgtt	367
15	5'- caagatgggcttttctcacc 5'- aagaaggcccagaccagag	379
16	5'- ccttagcgtctctgctgctt 5'- ctagcagccccatttgtctt	383
17+18	5'- aggaggagaaggccagaaag 5'- gatgatccagggaaagtgga	490
19	5'- tcacagcagccctgtgatac 5'- gtgggcacaagatgtgtcat	490
20	5'- aggaagccccctcaagtatg 5'- gcaggaaaggaaagggtagg	479
21	5'- gcagaaaggccagtgtcttc 5'- cctttggtcccttgtcttca	471
22	5'- tatccatgtgcctggcatta 5'- atgcaaagacacgcaaatca	482
23	5'- aatgatgcgcatttgtgtgt 5'- cttaccgtgtggccaagatt	388
24	5'- cgctcctctggagtcaagtc 5'- gctggtggtagaaggtggag	483
25	5'- cagagagatgggatgcgttt 5'- gacgaggtgtatgtgcctga	427

Supplementary Table 4. Primary Antibodies Used in this Study

Antigen protein	IF / IHC	FC	Clone	Source / Company
β-catenin	+		polyclonal	Abcam
CD3	+		F7.2.38	DAKO
CD4	+		4B12	DAKO
CD8	+		C8/144B	DAKO
CD20	+		L26	DAKO
CD68	+		KP1	DAKO
Collagen IV	+		C IV 22	Abcam
Collagen VII	+		LH7.2	Calbiochem
Collagen XVII	+		polyclonal	see Ref [11]
Fibronectin	+		ab2413	Abcam
Integriņ β1		+	4B7R	Abcam
Integriņ β1	+		B3B11	Chemicon
Integrin α3	+	+	P1B5	Chemicon
Integrin α2		+	16B4	Abcam
Integrin α6	+	+	GoH3	Progen
Integrin β4	+		3E1	Millipore
Keratin 14	+		LL002	DCS Hamburg
Keratin 10	+		LH2	Santa Cruz Biotechnology
Ki67	+		MIB-1	DAKO
Laminin α3	+		BM165	gift of B. Burgeson, Boston
Laminin β3	+		6F12	Santa Cruz Biotechnology
Laminin γ2	+		GB3	gift of G. Meneguzzi, Nice
Laminin α5	+		So4C7	gift of L. Sorokin, Münster
Pro-surfactant protein C	+		polyclonal	Millipore
Tenascin C	+		578	R&D Systems

Legend: +, used for the application; IF, immunofluorescence; IHC, immunohistochemistry; FC, flow cytometry.

SUPPLEMENTARY FIGURES

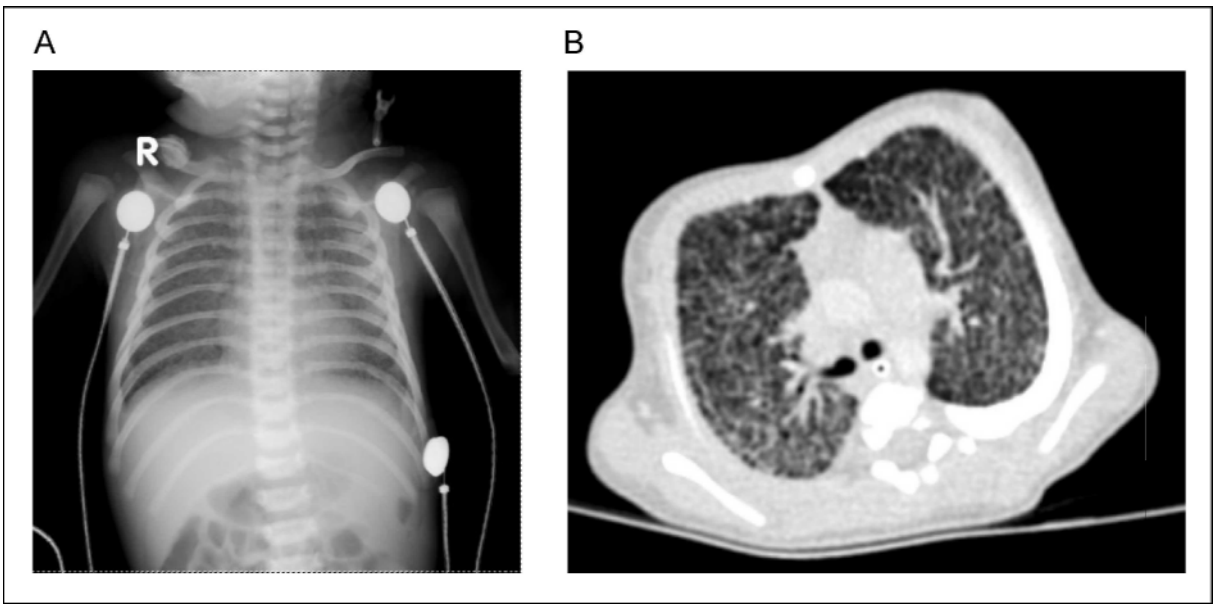

Supplementary Figure 1. Chest Radiograph and CT of Patient 2.

Panel A shows chest radiograph at 6 weeks, and panel B shows CT of the chest. Both demonstrate diffuse interstitial changes with inter- and intralobular septal thickening.

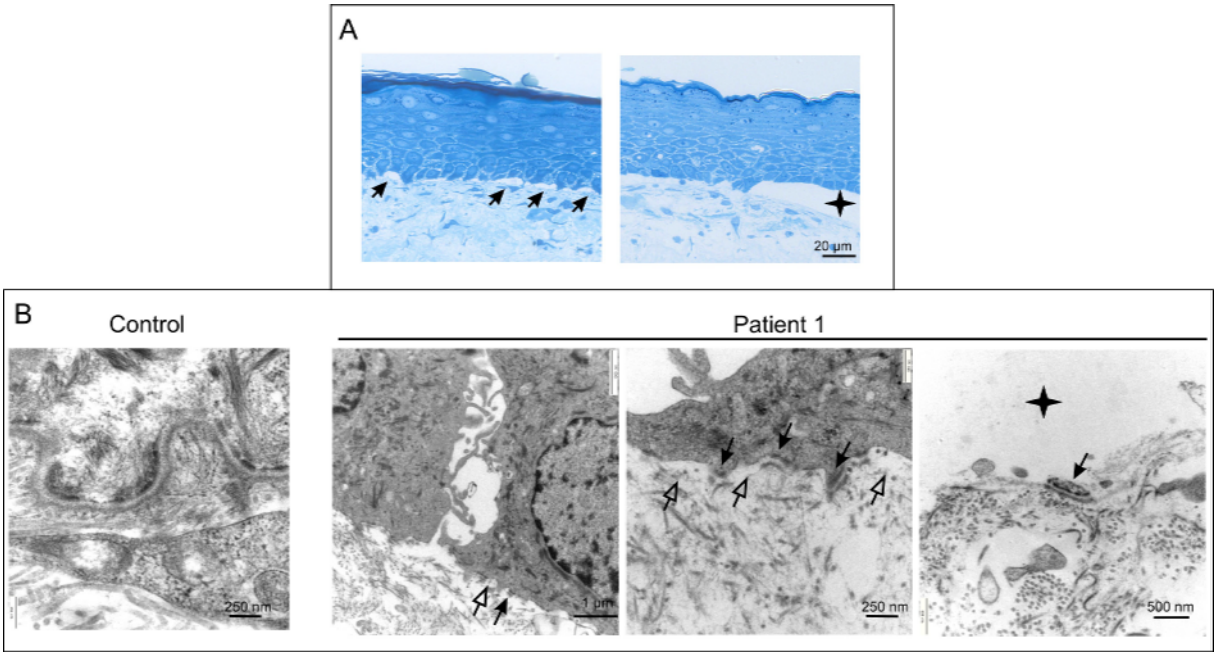

Supplementary Figure 2. Morphologic Features of the Skin of Patient 1. In panel A, semithin sections of a skin specimen of the patient are stained with methylene blue. Light microscopy of non-blistered skin reveals a flattened epidermis and microblisters (left panel, arrows). In blistered skin, subepidermal cleavage is seen (right panel, asterisk). Panels B show transmission electron microscopy of the dermal-epidermal junction in the patient and a control. In control skin, the lamina densa appears as a strong continuous line. In the patient´s skin, the lamina densa is very thin and discontinuous, and basal keratinocytes seem to detach from it. The lamina densa is present beneath the hemidesmosomes (black arrows), but interrupted in between (open arrows). The right panel shows occasional hemidesmosomes (arrow) on the blister floor, indicating intracellular rupture. The asterisk denotes the blister cavity.

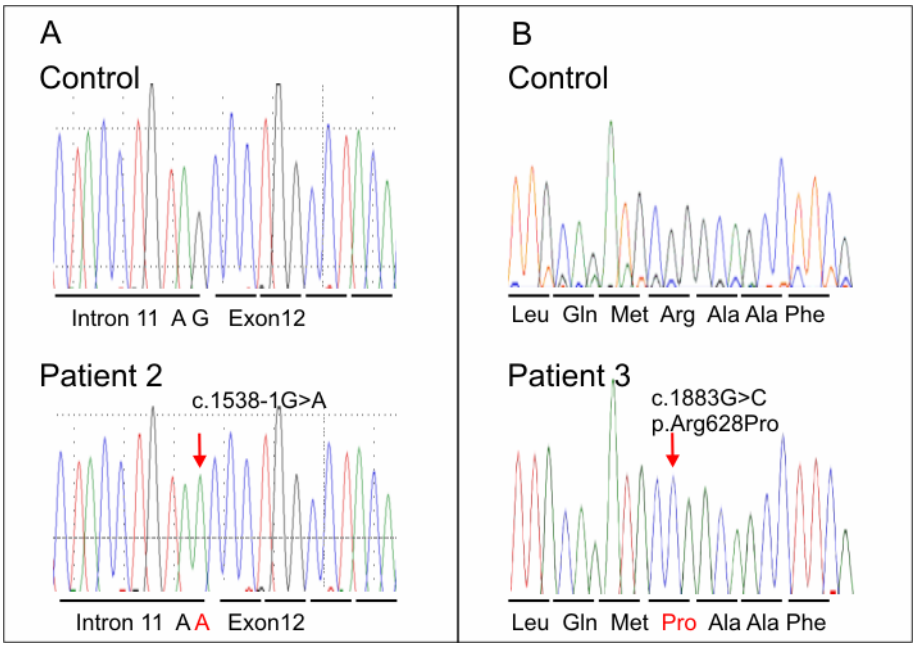

Supplementary Figure 3. Identification of *ITGA3* Mutations in Patients 2 and 3.

In both panels chromatograms reveal partial sequences of the *ITGA3* gene in controls and patients. In panel A, the homozygous mutation c.1538-1G>A (arrow) found in Patient 2 affects the position -1 of the obligatory acceptor splice site of exon 12. Panel B shows the missense mutation c.1883G>C, p. Arg628Pro (arrow) identified in Patient 3 in a homozygous state.

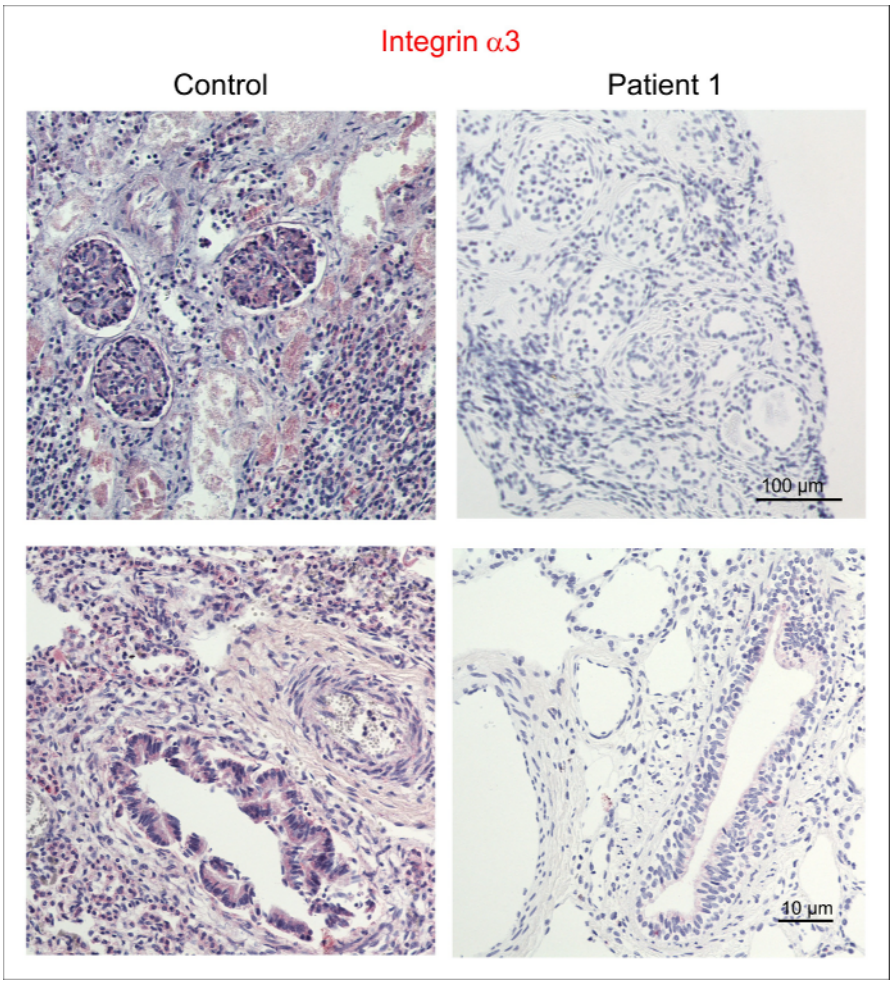

Supplementary Figure 4. Expression of Integrin α3 in Kidney and Lung.

Immunohistochemistry of integrin α3 in kidney (upper panels) and lung (lower panels) of a control subject and Patient 1, demonstrating loss of integrin α3 expression in the patient's samples.

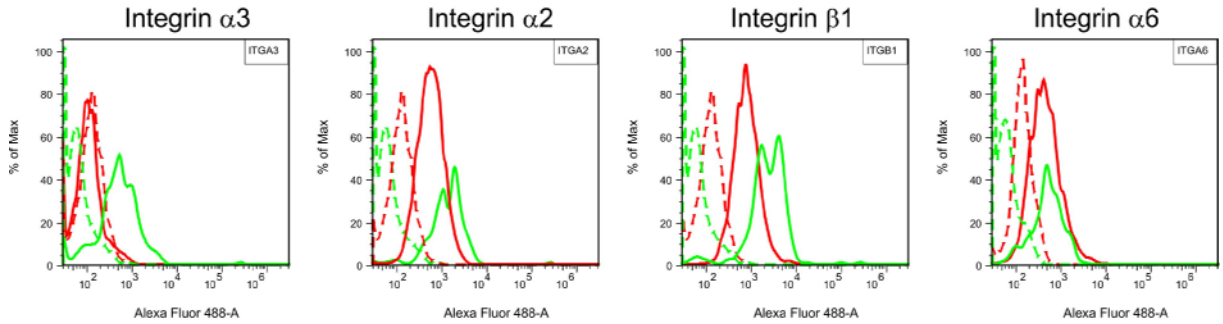

Supplementary Figure 5. Consequences of the *ITGA3* Deletion Mutation in Keratinocytes of Patient 1. Flow cytometry of keratinocytes from the Patient 1 (red curves), and a control (green curves), with antibodies to integrins α3, α2, β1 and α6 (continuous lines), or with secondary antibodies alone as a control (interrupted lines). It demonstrates complete absence of integrin α3 on the surface of keratinocytes derived from the patient, whereas integrins α2, β1 and α6 are not significantly altered.

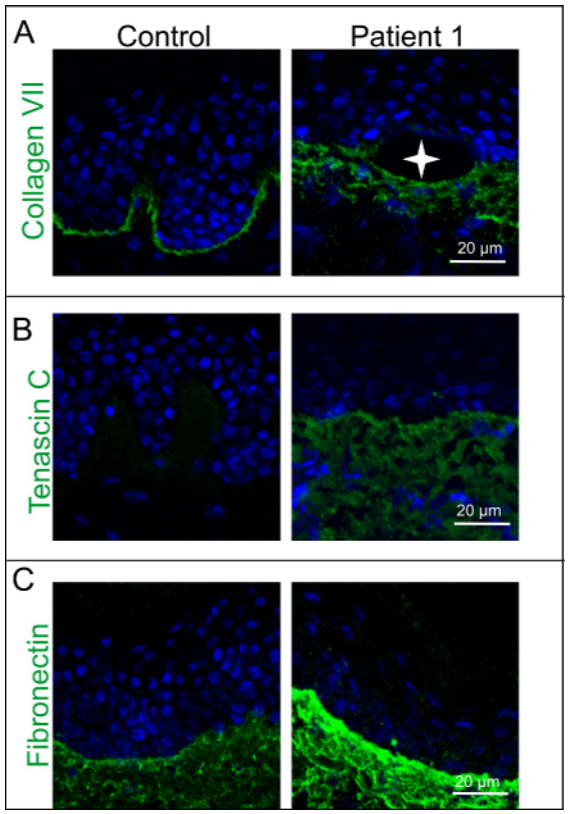

Supplementary Figure 6. Extracellular Matrix Proteins in the Skin of Patient 1.

Immunofluorescence staining is shown. Panel A shows a linear signal of collagen VII at the dermal-epidermal junction in control skin, but irregular distribution in the papillary dermis at the blister (asterisk) base in patient 1. In panels B and C, strong deposition of tenascin C and fibronectin is shown in the skin of the patient. Nuclei are visualized in blue with DAPI.

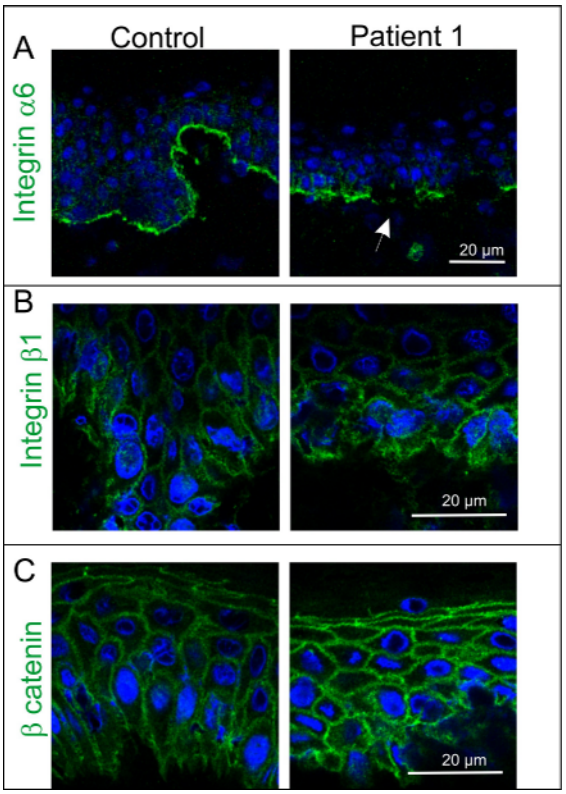

Supplementary Figure 7. Integrins and Cell-Cell Contacts in the Skin of Patient 1.

Immunofluorescence staining is shown. Panel A shows integrin α6 in the skin of a control and Patient 1. Loss of integrin α3 leads to discontinuous and irregular distribution of α6 integrin (arrow). Panel B shows similar integrin β1 patterns in control and the patient's skin. In panel C, β-catenin is used to delineate cell membranes. Note the regular, columnar shape of basal keratinocytes in normal skin. In contrast, in the patient´s skin the morphology of basal keratinocytes is clearly irregular.

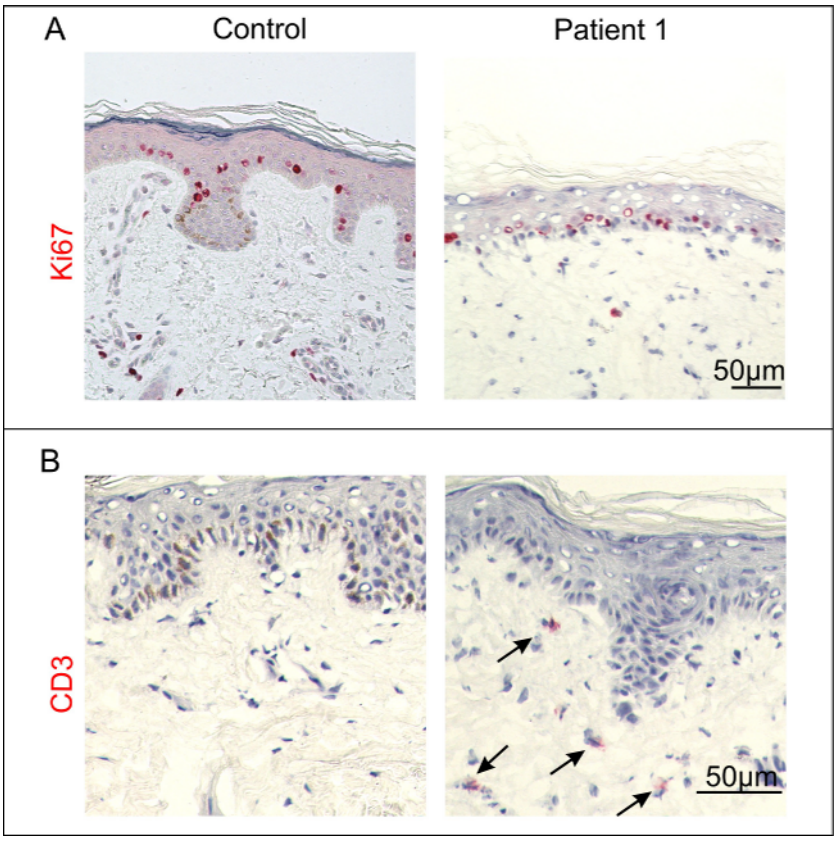

Supplementary Figure 8. Keratinocyte Proliferation and CD3 Positive Cells in the Skin of Patient 1.

Panels A show immunohistochemistry of Ki67 in the skin of an age-matched control and the patient. Note comparable staining patterns, demonstrating that keratinocyte proliferation is not hampered in the absence of integrin $\alpha 3$. In panel B, immunohistochemistry of CD3 reveals few inflammatory cells in the skin of the patient (arrows), whereas control skin remains negative.

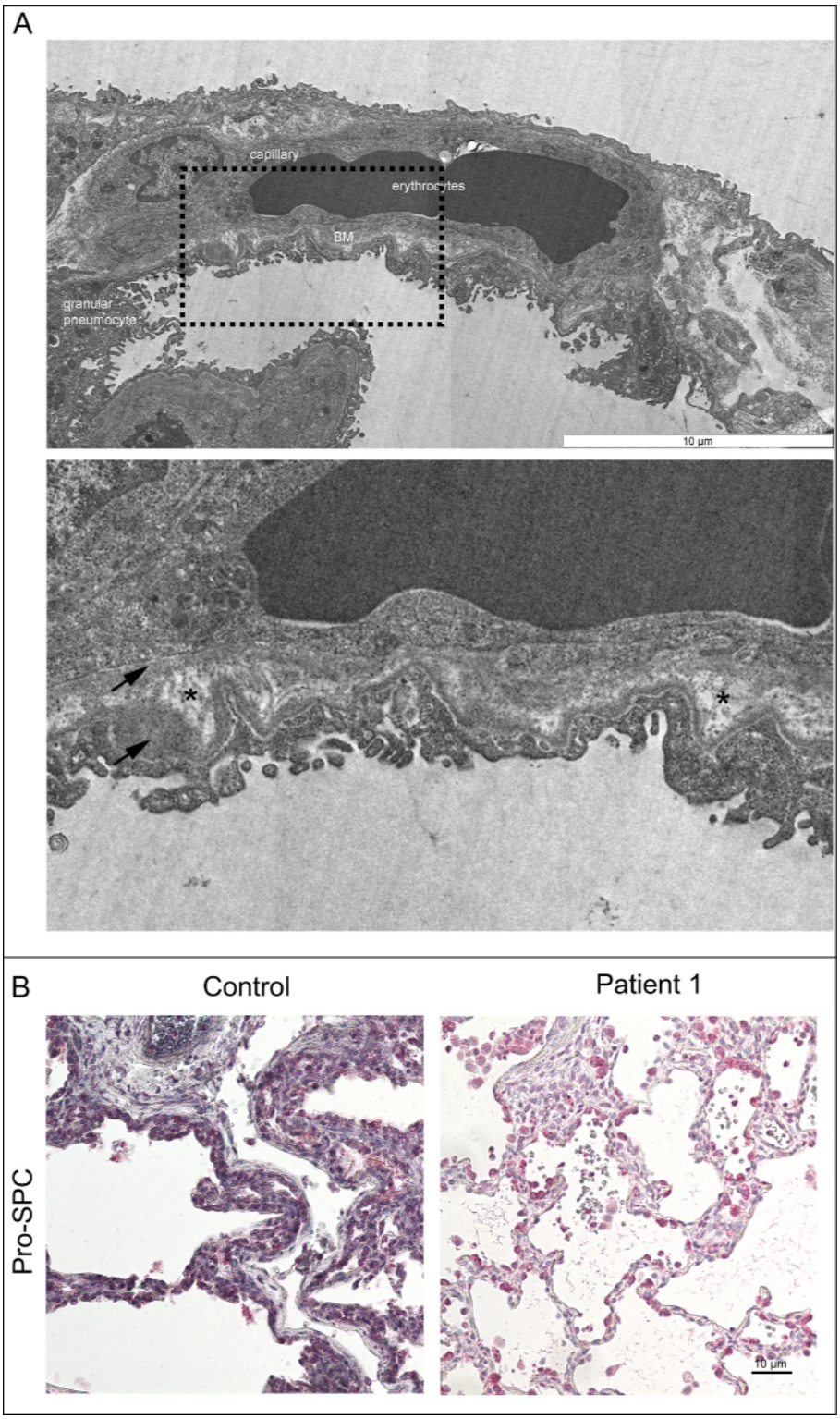

Supplementary Figure 9. Alveolar Basement Membrane and Pro-SPC in the Lung of Patient 1.

Panel A shows an electron micrograph representing the blood-air barrier with a capillary filled with erythrocytes, the basement membrane (BM) and pneumocytes. The lower panel is a 3-

fold magnification of the marked area in the upper panel. Note the irregular thickness (arrows) and splitting of the alveolar basement membrane (asterisk). In panel B, immunohistochemistry demonstrates abundant pro-SPC-positive type II alveolar cells.

REFERENCES

1. Otto EA, Hurd TW, Airik R, et al. Candidate exome capture identifies mutation of SDCCAG8 as the cause of a retinal-renal ciliopathy. Nat Genet 2010;42:840-50.
2. Karle SM, Uetz B, Ronner V, Glaeser L, Hildebrandt F, Fuchshuber A. Novel mutations in NPHS2 detected in both familial and sporadic steroid-resistant nephrotic syndrome. J Am Soc Nephrol 2002;13:388-93.
3. Otto E, Hoefele J, Ruf R, et al. A gene mutated in nephronophthisis and retinitis pigmentosa encodes a novel protein, nephroretinin, conserved in evolution. Am J Hum Genet 2002;71:1161-7.
4. Mucha B, Ozaltin F, Hinkes BG, et al. Mutations in the Wilms' tumor 1 gene cause isolated steroid resistant nephrotic syndrome and occur in exons 8 and 9. Pediatr Res 2006;59:325-31.
5. Shulenin S, Nogee LM, Annilo T, Wert SE, Whitsett JA, Dean M. ABCA3 gene mutations in newborns with fatal surfactant deficiency. N Engl J Med 2004;350:1296-303.
6. Has C, Herz C, Zimina E, et al. Kindlin-1 Is required for RhoGTPase-mediated lamellipodia formation in keratinocytes. Am J Pathol 2009;175:1442-52.
7. Symington BE, Carter WG. Modulation of epidermal differentiation by epiligrin and integrin alpha 3 beta 1. J Cell Sci 1995;108 (Pt 2):831-8.
8. Choma DP, Pumiglia K, DiPersio CM. Integrin alpha3beta1 directs the stabilization of a polarized lamellipodium in epithelial cells through activation of Rac1. J Cell Sci 2004;117:3947-59.
9. Margadant C, Raymond K, Kreft M, Sachs N, Janssen H, Sonnenberg A. Integrin alpha3beta1 inhibits directional migration and wound re-epithelialization in the skin. J Cell Sci 2009;122:278-88.
10. Kim KK, Wei Y, Szekeres C, et al. Epithelial cell alpha3beta1 integrin links beta-catenin and Smad signaling to promote myofibroblast formation and pulmonary fibrosis. J Clin Invest 2009;119:213-24.
11. Schacke H, Schumann H, Hammami-Hauasli N, Raghunath M, Bruckner-Tuderman L. Two forms of collagen XVII in keratinocytes. A full-length transmembrane protein and a soluble ectodomain. J Biol Chem 1998;273:25937-43.